


Springer Tracts in Mechanical Engineering

Tianjian Lu  
Fengxian Xin

# Vibro-Acoustics of Lightweight Sandwich Structures

 Science Press  
Beijing

 Springer

# **Springer Tracts in Mechanical Engineering**

For further volumes:

<http://www.springer.com/series/11693>



Tianjian Lu • Fengxian Xin

# Vibro-Acoustics of Lightweight Sandwich Structures

 Science Press  
Beijing

 Springer

Tianjian Lu  
Fengxian Xin  
Xi'an Jiaotong University  
Xi'an  
China

ISSN 2195-9862

ISBN 978-3-642-55357-8

DOI 10.1007/978-3-642-55358-5

Springer Heidelberg New York Dordrecht London

ISSN 2195-9870 (electronic)

ISBN 978-3-642-55358-5 (eBook)

Jointly published with Science Press, Beijing  
ISBN: 978-7-03-041322-2 Science Press, Beijing

Library of Congress Control Number: 2014942660

© Science Press Beijing and Springer-Verlag Berlin Heidelberg 2014

This work is subject to copyright. All rights are reserved by the Publishers, whether the whole or part of the material is concerned, specifically the rights of translation, reprinting, reuse of illustrations, recitation, broadcasting, reproduction on microfilms or in any other physical way, and transmission or information storage and retrieval, electronic adaptation, computer software, or by similar or dissimilar methodology now known or hereafter developed. Exempted from this legal reservation are brief excerpts in connection with reviews or scholarly analysis or material supplied specifically for the purpose of being entered and executed on a computer system, for exclusive use by the purchaser of the work. Duplication of this publication or parts thereof is permitted only under the provisions of the Copyright Law of the Publishers' locations, in its current version, and permission for use must always be obtained from Springer. Permissions for use may be obtained through RightsLink at the Copyright Clearance Center. Violations are liable to prosecution under the respective Copyright Law.

The use of general descriptive names, registered names, trademarks, service marks, etc. in this publication does not imply, even in the absence of a specific statement, that such names are exempt from the relevant protective laws and regulations and therefore free for general use.

While the advice and information in this book are believed to be true and accurate at the date of publication, neither the authors nor the editors nor the publishers can accept any legal responsibility for any errors or omissions that may be made. The publishers make no warranty, express or implied, with respect to the material contained herein.

Printed on acid-free paper

Springer is part of Springer Science+Business Media ([www.springer.com](http://www.springer.com))

# Preface

The purpose of this book is to present the vibration and acoustical behavior of typical sandwich structures subject to mechanical and/or acoustical loadings, which actually form a class of structural elements of practical importance in huge amounts of engineering applications, such as aircraft fuselage, ship and submarine hulls. The contents of this book has grown out of the research activities of the authors in the field of sound radiation/transmission of/through lightweight sandwich structures.

The book is organized into six chapters: Chapter 1 deals with the vibro-acoustic performance of rectangular multiple-panel partitions with enclosed air cavity theoretically and experimentally, which has accounted for the simply supported and clamp supported boundary conditions. Chapter 2 concerns with the transmission of external jet-noise through a uniform skin plate of aircraft cabin fuselage in the presence of external mean flow. As an extension, Chap. 3 handles with the noise radiation and transmission from/through aeroelastic skin plates of aircraft fuselage stiffened by orthogonally distributed rib-stiffeners in the presence of convected mean flow. Chapter 4 develops a theoretical model for sound transmission through all-metallic, two-dimensional, periodic sandwich structures having corrugated core. Chapter 5 focuses on the sound radiation and transmission characteristics of periodically stiffened structures. Ultimately, Chap. 6 proposes the sound radiation and transmission behaviors of periodical sandwich structures having cavity-filling fibrous sound absorptive materials.

This book is involving multidisciplinary subjects especially including combined knowledge of vibration, aeroelastics and structural acoustics, which pays much attention on showing results and conclusions, in addition to mere theoretical modelling. Therefore this book should be of considerable interest to a wide range of readers in relevant fields. It is hoped that the content of the book will find application not only as a textbook for a wide audience of engineering students, but also a general reference for researchers in the field of vibrations and acoustics.

Xi'an, China

T.J. Lu  
F.X. Xin



# Acknowledgements

Although the contents of this book has grown out of the research activities of the authors, we would also like to deeply appreciate the reproduction permission for figures, tables etc. from Elsevier, AIAA, ASME, Acoustical Society of America and Taylor & Francis Ltd. These research activities are supported by the National Basic Research Program of China (Grant No. 2011CB610300), the National Natural Science Foundation of China (Grant Nos. 11102148, and 11321062) and the Fundamental Research Funds for Central Universities (xjj2011005).





# Contents

<b>1</b>	<b>Transmission of Sound Through Finite Multiple-Panel Partition</b> .....	<b>1</b>
1.1	Simply Supported Finite Double-Panel Partitions .....	2
1.1.1	Introduction .....	2
1.1.2	Vibroacoustic Theoretical Modeling .....	4
1.1.3	Mathematic Formulation and Solution .....	5
1.1.4	Convergence Check for Numerical Results .....	10
1.1.5	Model Validation .....	11
1.1.6	Effects of Air Cavity Thickness .....	13
1.1.7	Effects of Panel Dimensions .....	17
1.1.8	Effects of Incident Elevation Angle and Azimuth Angle ....	20
1.1.9	Conclusions .....	23
1.2	Clamped Finite Double-Panel Partitions .....	24
1.2.1	Introduction .....	24
1.2.2	Modeling of the Vibroacoustic Coupled System.....	26
1.2.3	Model Validation .....	32
1.2.4	Finite Versus Infinite Double-Panel Partition .....	34
1.2.5	Effects of Panel Thickness on STL .....	35
1.2.6	Effects of Air Cavity Thickness on STL .....	37
1.2.7	Effects of Incident Angles on STL .....	37
1.2.8	Conclusions .....	40
1.2.9	Sound Transmission Measurements .....	41
1.2.10	Relationships Between Clamped and Simply Supported Boundary Conditions.....	47
1.2.11	Conclusions .....	51
1.3	Clamped Finite Triple-Panel Partitions .....	53
1.3.1	Introduction .....	53
1.3.2	Dynamic Structural Acoustic Formulation .....	56
1.3.3	The Principle of Virtual Work .....	60
1.3.4	Determination of Modal Coefficients .....	60
1.3.5	Sound Transmission Loss .....	63
1.3.6	Model Validation .....	63

1.3.7	Physical Interpretation of STL Dips .....	64
1.3.8	Comparison Among Single-, Double-, and Triple-Panel Partitions with Equivalent Total Mass .....	68
1.3.9	Asymptotic Variation of STL Versus Frequency Curve from Finite to Infinite System .....	69
1.3.10	Effects of Panel Thickness .....	70
1.3.11	Effects of Air Cavity Depth .....	74
1.3.12	Concluding Remarks .....	75
Appendices .....		77
Appendix A .....		77
Appendix B .....		80
References .....		83
<b>2</b>	<b>Vibroacoustics of Uniform Structures in Mean Flow .....</b>	<b>87</b>
2.1	Finite Single-Leaf Aeroelastic Plate .....	88
2.1.1	Introduction .....	88
2.1.2	Modeling of Aeroelastic Coupled System .....	90
2.1.3	Effects of Mean Flow in Incident Field .....	99
2.1.4	Effects of Mean Flow in Transmitted Field .....	103
2.1.5	Effects of Incident Elevation Angle in the Presence of Mean Flow on Both Incident Side and Transmitted Side .....	106
2.1.6	Conclusions .....	108
2.2	Infinite Double-Leaf Aeroelastic Plates .....	109
2.2.1	Introduction .....	109
2.2.2	Statement of the Problem .....	111
2.2.3	Formulation of Plate Dynamics .....	112
2.2.4	Consideration of Fluid-Structure Coupling .....	114
2.2.5	Definition of Sound Transmission Loss .....	117
2.2.6	Characteristic Impedance of an Infinite Plate .....	117
2.2.7	Physical Interpretation for the Appearance of STL Peaks and Dips .....	119
2.2.8	Effects of Mach Number .....	122
2.2.9	Effects of Elevation Angle .....	127
2.2.10	Effects of Azimuth Angle .....	128
2.2.11	Effects of Panel Curvature and Cabin Internal Pressurization .....	129
2.2.12	Conclusions .....	130
2.3	Double-Leaf Panel Filled with Porous Materials .....	131
2.3.1	Introduction .....	131
2.3.2	Problem Description .....	133
2.3.3	Theoretical Model .....	134
2.3.4	Validation of Theoretical Model .....	140
2.3.5	Influence of Porous Material and the Faceplates .....	141
2.3.6	Influence of Porous Material Layer Thickness .....	143

2.3.7	Influence of External Mean Flow .....	144
2.3.8	Influence of Incident Sound Elevation Angle .....	147
2.3.9	Influence of Sound Incident Azimuth Angle .....	148
2.3.10	Conclusion .....	150
Appendix	.....	151
Mass-Air-Mass Resonance	.....	151
Standing-Wave Attenuation	.....	152
Standing-Wave Resonance	.....	152
Coincidence Resonance	.....	153
References	.....	154
<b>3</b>	<b>Vibroacoustics of Stiffened Structures in Mean Flow</b> .....	<b>159</b>
3.1	Noise Radiation from Orthogonally Rib-Stiffened Plates .....	160
3.1.1	Introduction .....	160
3.1.2	Theoretical Formulation .....	162
3.1.3	Effect of Mach Number .....	170
3.1.4	Effect of Incidence Angle .....	172
3.1.5	Effect of Periodic Spacings .....	173
3.1.6	Concluding Remarks .....	175
3.2	Transmission Loss of Orthogonally Rib-Stiffened Plates .....	176
3.2.1	Introduction .....	176
3.2.2	Theoretical Formulation .....	178
3.2.3	Model Validation .....	187
3.2.4	Effects of Mach Number of Mean Flow .....	189
3.2.5	Effects of Rib-Stiffener Spacings .....	190
3.2.6	Effects of Rib-Stiffener Thickness and Height .....	193
3.2.7	Effects of Elevation and Azimuth Angles of Incident Sound .....	194
3.2.8	Conclusions .....	197
Appendices	.....	198
Appendix A	.....	198
Appendix B	.....	201
References	.....	203
<b>4</b>	<b>Sound Transmission Across Sandwich Structures with Corrugated Cores</b> .....	<b>207</b>
4.1	Introduction .....	207
4.2	Development of Theoretical Model .....	209
4.3	Effects of Core Topology on Sound Transmission Across the Sandwich Structure .....	214
4.4	Physical Interpretation for the Existence of Peaks and Dips on STL Curves .....	215
4.5	Optimal Design for Combined Sound Insulation and Structural Load Capacity .....	219
4.6	Conclusion .....	220
References	.....	221

<b>5</b>	<b>Sound Radiation, Transmission of Orthogonally Rib-Stiffened Sandwich Structures</b> .....	225
5.1	Sound Radiation of Sandwich Structures .....	226
5.1.1	Introduction .....	226
5.1.2	Theoretical Modeling of Structural Dynamic Responses ....	228
5.1.3	Solutions .....	234
5.1.4	Far-Field Radiated Sound Pressure .....	238
5.1.5	Validation of Theoretical Modeling .....	239
5.1.6	Influences of Inertial Effects Arising from Rib-Stiffener Mass .....	240
5.1.7	Influence of Excitation Position .....	242
5.1.8	Influence of Rib-Stiffener Spacings .....	243
5.1.9	Conclusions .....	244
5.2	Sound Transmission Through Sandwich Structures .....	245
5.2.1	Introduction .....	245
5.2.2	Analytic Formulation of Panel Vibration and Sound Transmission .....	248
5.2.3	The Acoustic Pressure and Continuity Condition .....	257
5.2.4	Solution of the Formulations with the Virtual Work Principle .....	258
5.2.5	Virtual Work of Panel Elements .....	259
5.2.6	Virtual Work of $x$ -Wise Rib-Stiffeners .....	260
5.2.7	Virtual Work of $y$ -Wise Rib-Stiffeners .....	261
5.2.8	Combination of Equations .....	261
5.2.9	Definition of Sound Transmission Loss .....	264
5.2.10	Convergence Check for Space-Harmonic Series Solution ..	265
5.2.11	Validation of the Analytic Model .....	266
5.2.12	Influence of Sound Incident Angles .....	267
5.2.13	Influence of Inertial Effects Arising from Rib-Stiffener Mass .....	269
5.2.14	Influence of Rib-Stiffener Spacings .....	270
5.2.15	Influence of Airborne and Structure-Borne Paths .....	271
5.2.16	Conclusions .....	272
	Appendices .....	273
	Appendix A .....	273
	Appendix B .....	278
	References .....	285
<b>6</b>	<b>Sound Propagation in Rib-Stiffened Sandwich Structures with Cavity Absorption</b> .....	289
6.1	Sound Radiation of Absorptive Sandwich Structures .....	290
6.1.1	Introduction .....	290
6.1.2	Structural Dynamic Responses to Time-Harmonic Point Force .....	292
6.1.3	The Acoustic Pressure and Fluid-Structure Coupling .....	295

6.1.4	Far-Field Sound-Radiated Pressure .....	300
6.1.5	Convergence Check for Numerical Solution .....	300
6.1.6	Validation of Theoretical Modeling .....	301
6.1.7	Influence of Air-Structure Coupling Effect .....	303
6.1.8	Influence of Fibrous Sound Absorptive Filling Material ....	305
6.1.9	Conclusions .....	307
6.2	Sound Transmission Through Absorptive Sandwich Structure .....	308
6.2.1	Introduction .....	308
6.2.2	Analytic Formulation of Panel Vibration and Sound Transmission .....	309
6.2.3	Application of the Periodicity of Structures.....	313
6.2.4	Solution by Employing the Virtual Work Principle.....	316
6.2.5	Model Validation .....	321
6.2.6	Effects of Fluid-Structure Coupling on Sound Transmission.....	322
6.2.7	Sound Transmission Loss Combined with Bending Stiffness and Structure Mass: Optimal Design of Sandwich .....	324
6.2.8	Conclusions .....	327
Appendices	.....	328
Appendix A	.....	328
Appendix B	.....	330
Appendix C	.....	333
References	.....	338

# Chapter 1

## Transmission of Sound Through Finite Multiple-Panel Partition

**Abstract** This chapter is organized as three parts: in the first part, the vibroacoustic performance of a rectangular double-panel partition with enclosed air cavity and simply mounted on an infinite acoustic rigid baffle is investigated analytically. The sound velocity potential method rather than the commonly used cavity modal function method is employed, which possesses good expandability and has significant implications for further vibroacoustic investigations. The simply supported boundary condition is accounted for by using the method of modal function, and double Fourier series solutions are obtained to characterize the vibroacoustic behaviors of the structure. Results for sound transmission loss (STL), panel vibration level, and sound pressure level are presented to explore the physical mechanisms of sound energy penetration across the finite double-panel partition. Specifically, focus is placed upon the influence of several key system parameters on sound transmission, including the thickness of air cavity, structural dimensions, and the elevation angle and azimuth angle of the incidence sound. Further extensions of the sound velocity potential method to typical framed double-panel structures are also proposed.

In the second part, the air-borne sound insulation performance of a rectangular double-panel partition clamp mounted on an infinite acoustic rigid baffle is investigated both analytically and experimentally, and compared with that of a simply supported one. With the clamped (or simply supported) boundary accounted for by using the method of modal function, a double series solution for the sound transmission loss (*STL*) of the structure is obtained by employing the weighted residual (Galerkin) method. Experimental measurements with Al double-panel partitions having air cavity are subsequently carried out to validate the theoretical model for both types of the boundary condition, and good overall agreement is achieved. A consistency check of the two different models (based separately on clamped modal function and simply supported modal function) is performed by

extending the panel dimensions to infinite where no boundaries exist. The significant discrepancies between the two different boundary conditions are demonstrated in terms of the *STL* versus frequency plots as well as the panel deflection mode shapes.

In the third part, an analytical model for sound transmission through a clamped triple-panel partition of finite extent and separated by two impervious air cavities is formulated. The solution derived from the model takes the form of that for a clamp-supported rectangular plate. A set of modal functions (or more strictly speaking, the basic functions) are employed to account for the clamped boundary conditions, and the application of the virtual work principle leads to a set of simultaneous algebraic equations for determining the unknown modal coefficients. The sound transmission loss (*STL*) of the triple-panel partition as a function of excitation frequency is calculated and compared with that of a double-panel partition. The model predictions are then used to explore the physical mechanisms associated with the various dips on the *STL* versus frequency curve, including the equivalent “mass-spring” resonance, the standing-wave resonance, and the panel modal resonance. The asymptotic variation of the solution from a finite-sized partition to an infinitely large partition is illustrated in such a way as to demonstrate the influence of the boundary conditions on the soundproofing capability of the partition. In general, a triple-panel partition outperforms a double-panel partition in insulating the incident sound, and the relatively large number of system parameters pertinent to the triple-panel partition in comparison with that of the double-panel partition offers more design space for the former to tailor its noise reduction performance.

## 1.1 Simply Supported Finite Double-Panel Partitions

### 1.1.1 Introduction

Double-leaf partition structures have found increasingly wide applications in noise control engineering due to their superior sound insulation capability over single-leaf configurations. Typical examples include transportation vehicles, grazing windows and partition walls in buildings, aircraft fuselage shells, and so on [1–12].

Considerable efforts have been devoted to understanding and predicting the transmission of sound across single-leaf [13–15] and double-leaf [16–29] partitions. In fact, research about the former is often a prerequisite for studying the latter. For instance, Lomas [14] developed Green function solution for the steady-state vibration of an elastically supported rectangular plate coupled to a semi-infinite acoustic medium. An important feature of the investigation is the treatment of the elastic support boundary condition which was taken into account by assuming the rotational motion along the boundary controlled by distributions of massless



rotary springs and by introducing the corresponding moments into the governing equations. The problem of sound radiation by a simply supported unbaffled panel was investigated by Laulagnet [13]. Both pressure jump and plate displacement in series of the simply supported plate models were developed.

Early sound transmission studies [16, 28–30] of double-panel structures with air cavity in between generally simplified the structure as infinite and hence did not account for the elastic boundary conditions on the periphery. For typical examples, Antonio et al. [17] gave an analytical evaluation of the acoustic insulation provided by double infinite walls and also did not take elastic boundary condition into account. Kropp et al. [19] addressed the optimization of sound insulation of double-panel constructions by dividing the frequency range into three cases, i.e., where the double wall resonance frequency is much higher (or closer or much lower) than the critical frequency of the total construction. Recently, Tadeu et al. [20] adopted an analytical method to assess the airborne sound and impact insulation properties of single- and double-leaf panels by neglecting the elastic boundary conditions. Bao and Pan [31] presented an experimental study on active control of sound transmission through double walls with different approaches, including cavity control, panel control, and room control.

For simply supported, finite rectangular double-panel structures, existing studies [3, 22–27, 32–37] concerned mainly with the loss of sound transmission across the structure, without detailed analysis about the energy transmission, the vibroacoustic coupling effects, and the physical mechanisms of sound transmission process across the structure. In particular, previous studies on double-panel partitions focus on either infinite extent or finite extent, without exploring the natural relationship between the two. The present study squarely addresses these deficiencies from the new perspectives of the integration analysis of STL, panel vibration level, and sound pressure level, with more details and the physical nature of sound penetration through double-panel partitions revealed. Since the rigid baffle bounds the cavity as well as the panel so that the cavity boundaries restrict the field to sinusoidal distributions parallel to the panel plane, analytical solutions in double Fourier series are proposed by applying the sinusoidal distributed sound velocity potential method. This method can be easily expanded to the vibroacoustic analysis of rib-stiffened double-panel structures, accounting for both the structure-borne route (i.e., structural connections between the two panels) and the airborne route (i.e., air cavity between the two panels), and hence can be regarded as an alternative of the cavity mode method in certain engineering applications. The model predictions are validated by comparing the analytical results with existing experimental data. The influences of key system parameters such as air cavity thickness, panel dimensions, and elevation angle and azimuth angle of incident sound on the sound insulation capability of the finite double-panel partition are systematically investigated. The results and conclusions of the present study should be referentially significant to others due to the similar physical nature of the vibroacoustic problem.

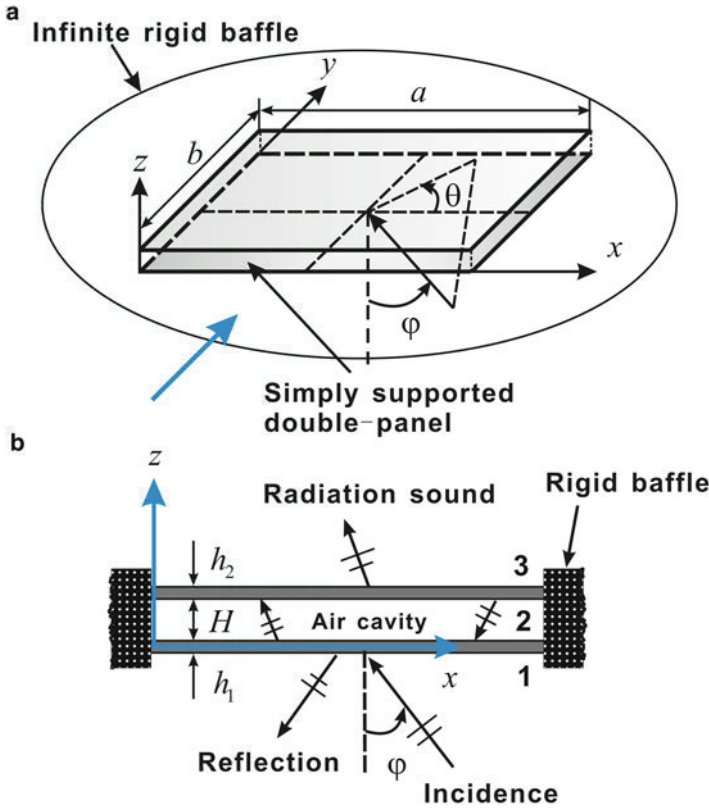


**Fig. 1.1** Schematic of sound transmission through a baffled, rectangular, simply supported double-panel partition: (a) global view; (b) side view in the *arrow direction* in (a) (With permission from ASME)

### 1.1.2 Vibroacoustic Theoretical Modeling

The finite double-panel partition with enclosed air cavity is assumed to be rectangular, baffled, and simply supported along its boundaries, as shown in Fig. 1.1. The two panels are homogenous and isotropic and modeled as classical thin plate. The following geometrical dimensions are considered: the incident (bottom) panel and the radiating (top) panel have identical length  $a$  and width  $b$ , but may have different thicknesses  $h_1$  and  $h_2$  (Fig. 1.1b); the thickness of the air cavity is  $H$  (Fig. 1.1b). The whole configuration is mounted on an infinite acoustic rigid baffle which separates the space into two fields, i.e., sound incidence field ( $z < 0$ ) and sound radiating field ( $z > H$ ). A uniform plane sound wave varying harmonically in time is obliquely incident on the bottom panel, with incident elevation angle  $\varphi$  and azimuth angle  $\theta$  (Fig. 1.1b). The vibration of the incident panel induced by the incident sound is transmitted through the enclosed air cavity to the radiating panel, which radiates

sound into the acoustic medium. The vibroacoustic behaviors of the double-panel structure coupling with air cavity as well as sound transmission loss across the structure are to be solved analytically with the sound velocity potential method.

### 1.1.3 Mathematic Formulation and Solution

For an obliquely incident uniform plane sound wave varying harmonically in time, its acoustic velocity potential can be expressed as

$$\phi = I e^{-j(k_x x + k_y y + k_z z - \omega t)} \quad (1.1)$$

where  $I$  is the amplitude;  $j = \sqrt{-1}$ ;  $\omega$  is the angular frequency; and  $k_x$ ,  $k_y$ , and  $k_z$  are the wavenumber components in the  $x$ -,  $y$ -, and  $z$ -directions, respectively:

$$k_x = k_0 \sin \varphi \cos \theta, \quad k_y = k_0 \sin \varphi \sin \theta, \quad k_z = k_0 \cos \varphi \quad (1.2)$$

Here,  $k_0 = \omega/c_0$  is the acoustic wavenumber in air, with  $c_0$  denoting the sound speed in air.

Due to the excitation of the incident sound wave, the double-panel configuration with enclosed air cavity vibrates and radiates sound. The vibroacoustic behaviors of the structure are governed by

$$D_1 \nabla^4 w_1 + m_1 \frac{\partial^2 w_1}{\partial t^2} - j\omega \rho_0 (\Phi_1 - \Phi_2) = 0 \quad (1.3)$$

$$D_2 \nabla^4 w_2 + m_2 \frac{\partial^2 w_2}{\partial t^2} - j\omega \rho_0 (\Phi_2 - \Phi_3) = 0 \quad (1.4)$$

where  $\rho_0$  is the air density and  $(w_1, w_2)$ ,  $(m_1, m_2)$  and  $(D_1, D_2)$  are the transverse displacements, surface densities, and flexural rigidities of the incident and radiating panels, located at  $z=0$  and  $z=H$ , respectively (Fig. 1.1). By introducing the loss factor of the panel material, the flexural rigidity of the panel  $D_i$  ( $i=1, 2$ ) can be written in terms of the complex Young's modulus  $E_i(1+j\eta_i)$  as

$$D_i = \frac{E_i h_i^3 (1 + j\eta_i)}{12 (1 - \nu_i^2)} \quad (1.5)$$

The hard-walled cavity modal function  $\phi_{mnl}^c = \cos(m\pi x/a)\cos(n\pi y/b)\cos(l\pi z/c)$  can only accurately model the sound field in a rigidly bounded cavity volume. It will therefore deviate somewhat from the precise results when the hard-walled cavity modal function is employed here to model the cavity bounded by two large flexural panels. In order to avoid this drawback, the sound velocity potential method is adopted, which is completely different from previous investigations based on cavity

modal function. Let  $\Phi_i$  ( $i = 1, 2, 3$ ) denote the velocity potentials of the three acoustic fields, i.e., sound incidence field, air cavity field, and structure radiating field (Fig. 1.1b), respectively. The velocity potential for the incident field can be defined as

$$\Phi_1(x, y, z; t) = Ie^{-j(k_x x + k_y y + k_z z - \omega t)} + \beta e^{-j(k_x x + k_y y - k_z z - \omega t)} \quad (1.6)$$

where the first and second terms represent separately the velocity potential of the incident and the reflected plus radiating sound waves and  $I$  and  $\beta$  are the amplitudes of the incident (i.e., positive-going) and the reflected plus radiating (i.e., negative-going) waves, respectively. Similarly, the velocity potential in the air cavity can be written as

$$\Phi_2(x, y, z; t) = \varepsilon e^{-j(k_x x + k_y y + k_z z - \omega t)} + \zeta e^{-j(k_x x + k_y y - k_z z - \omega t)} \quad (1.7)$$

where  $\varepsilon$  is the amplitude of positive-going wave and  $\zeta$  is the amplitude of negative-going wave. In the radiating field, there exist no reflected waves; thus, the velocity potential is only for radiating waves:

$$\Phi_3(x, y, z; t) = \xi e^{-j(k_x x + k_y y + k_z z - \omega t)} \quad (1.8)$$

where  $\xi$  is the amplitude of radiating (i.e., positive-going) wave. The local acoustic velocities and sound pressure are related to the velocity potentials by

$$\hat{\mathbf{u}}_i = -\nabla\Phi_i, \quad p_i = \rho_0 \frac{\partial\Phi_i}{\partial t} = j\omega\rho_0\Phi_i \quad (i = 1, 2, 3) \quad (1.9)$$

For simply supported boundary condition, the transverse displacement and the transverse force are constrained to be zero at the periphery of the panel. Given that the double-panel structure is rectangular, the boundary conditions can be expressed as

$$x = 0, a : \quad w_1 = w_2 = 0, \quad \frac{\partial^2 w_1}{\partial x^2} = \frac{\partial^2 w_2}{\partial x^2} = 0 \quad (1.10)$$

$$y = 0, b : \quad w_1 = w_2 = 0, \quad \frac{\partial^2 w_1}{\partial y^2} = \frac{\partial^2 w_2}{\partial y^2} = 0 \quad (1.11)$$

At the air-panel interface, the normal velocity should be continuous, yielding the following velocity compatibility equations:

$$z = 0 : \quad -\frac{\partial\Phi_1}{\partial z} = j\omega w_1, \quad -\frac{\partial\Phi_2}{\partial z} = j\omega w_1 \quad (1.12)$$

$$z = H : \quad -\frac{\partial\Phi_2}{\partial z} = j\omega w_2, \quad -\frac{\partial\Phi_3}{\partial z} = j\omega w_2 \quad (1.13)$$

For harmonic excitation of the finite double-panel system, the transverse displacements of the two panels can be written as

$$w_1(x, y, t) = \sum_{m=1}^{\infty} \sum_{n=1}^{\infty} \phi_{mn}(x, y) q_{1,mn}(t) \quad (1.14)$$

$$w_2(x, y, t) = \sum_{m=1}^{\infty} \sum_{n=1}^{\infty} \phi_{mn}(x, y) q_{2,mn}(t) \quad (1.15)$$

where the modal functions  $\phi_{mn}$  and modal displacements  $q_{i,mn}$  for simply supported boundary conditions (1.10) and (1.11) are given by

$$\phi_{mn}(x, y) = \sin \frac{m\pi x}{a} \sin \frac{n\pi y}{b} \quad (1.16)$$

$$q_{1,mn}(t) = \alpha_{1,mn} e^{j\omega t}, \quad q_{2,mn}(t) = \alpha_{2,mn} e^{j\omega t} \quad (1.17)$$

where  $\alpha_{1,mn}$  and  $\alpha_{2,mn}$  are the modal coefficients of the incident panel and the upper panel, respectively.

Since the rigid baffle bounds the cavity as well as the panel, the cavity boundaries restrict the field to sinusoidal distributions parallel to the panel plane. Therefore, the velocity potentials can be expressed in terms of the panel modal functions as

$$\begin{aligned} \Phi_1(x, y, z; t) &= \sum_{m=1}^{\infty} \sum_{n=1}^{\infty} I_{mn} \phi_{mn}(x, y) e^{-j(k_z z - \omega t)} \\ &\quad + \sum_{m=1}^{\infty} \sum_{n=1}^{\infty} \beta_{mn} \phi_{mn}(x, y) e^{-j(-k_z z - \omega t)} \end{aligned} \quad (1.18)$$

$$\begin{aligned} \Phi_2(x, y, z; t) &= \sum_{m=1}^{\infty} \sum_{n=1}^{\infty} \varepsilon_{mn} \phi_{mn}(x, y) e^{-j(k_z z - \omega t)} \\ &\quad + \sum_{m=1}^{\infty} \sum_{n=1}^{\infty} \zeta_{mn} \phi_{mn}(x, y) e^{-j(-k_z z - \omega t)} \end{aligned} \quad (1.19)$$

$$\Phi_3(x, y, z; t) = \sum_{m=1}^{\infty} \sum_{n=1}^{\infty} \xi_{mn} \phi_{mn}(x, y) e^{-j(k_z z - \omega t)} \quad (1.20)$$

where the unknown coefficients  $I_{mn}$ ,  $\beta_{mn}$ ,  $\varepsilon_{mn}$ ,  $\zeta_{mn}$ , and  $\xi_{mn}$  in (1.18), (1.19), and (1.20) can be determined by applying the orthogonality condition of the modal functions as

$$\tilde{\lambda}_{mn} = \frac{4}{ab} \int_0^b \int_0^a \tilde{\lambda} e^{-j(k_x x + k_y y)} \sin \frac{m\pi x}{a} \sin \frac{n\pi y}{b} dx dy \quad (1.21)$$

Here, the symbol  $\bar{\lambda}$  can be referred to any of the coefficients  $I$ ,  $\beta$ ,  $\varepsilon$ ,  $\zeta$ , and  $\xi$ . Note that the expressions in terms of either traveling wave or panel modal functions are completely equivalent in nature when they are both subjected to the same boundary conditions.

Substitution of Eqs. (1.18), (1.19), and (1.20) into Eqs. (1.12) and (1.13) leads to

$$\beta_{mn} = I_{mn} - \frac{\omega\alpha_{1,mn}}{k_z} \quad (1.22)$$

$$\varepsilon_{mn} = \frac{\omega(\alpha_{2,mn}e^{jk_zH} - \alpha_{1,mn}e^{2jk_zH})}{k_z(1 - e^{2jk_zH})} \quad (1.23)$$

$$\zeta_{mn} = \frac{\omega(\alpha_{2,mn}e^{jk_zH} - \alpha_{1,mn})}{k_z(1 - e^{2jk_zH})} \quad (1.24)$$

$$\xi_{mn} = \frac{\omega\alpha_{2,mn}e^{jk_zH}}{k_z} \quad (1.25)$$

Substituting Eqs. (1.14), (1.15), and (1.22), (1.23), (1.24), and (1.25) into Eqs. (1.3) and (1.4) and applying the orthogonal properties of modal functions, one gets

$$\ddot{q}_{1,kl}(t) + \omega_{1,kl}^2 q_{1,kl}(t) - \frac{j\omega\rho_0}{m_1} \left[ (I_{kl} - \varepsilon_{kl}) e^{-j(k_z z - \omega t)} + (\beta_{kl} - \zeta_{kl}) e^{-j(-k_z z - \omega t)} \right] = 0 \quad (1.26)$$

$$\ddot{q}_{2,kl}(t) + \omega_{2,kl}^2 q_{2,kl}(t) - \frac{j\omega\rho_0}{m_2} \left[ (\varepsilon_{kl} - \xi_{kl}) e^{-j(k_z z - \omega t)} + \zeta_{kl} e^{-j(-k_z z - \omega t)} \right] = 0 \quad (1.27)$$

where  $\omega_{i,kl}$  is defined as

$$\omega_{i,kl}^2 = \frac{D_i \iint \nabla^4 \phi_{i,kl} \cdot \phi_{i,kl} dx dy}{m_i \iint \phi_{i,kl}^2 dx dy} \quad (i = 1, 2) \quad (1.28)$$

With Eq. (1.17), Eqs. (1.26) and (1.27) can be rewritten in matrix form as

$$\begin{bmatrix} Q_{11} & Q_{12} \\ Q_{21} & Q_{22} \end{bmatrix} \begin{Bmatrix} \alpha_{1,kl} \\ \alpha_{2,kl} \end{Bmatrix} = \begin{Bmatrix} F \\ 0 \end{Bmatrix} \quad (1.29)$$

where

$$Q_{11} = \omega_{1,kl}^2 - \omega^2 - \frac{j\omega\rho_0}{m_1} \frac{2\omega e^{2jk_zH}}{k_z(1 - e^{2jk_zH})} \quad (1.30)$$

$$Q_{12} = \frac{j\omega\rho_0}{m_1} \frac{2\omega e^{jk_z H}}{k_z (1 - e^{2jk_z H})} \quad (1.31)$$

$$Q_{21} = \frac{j\omega\rho_0}{m_2} \frac{2\omega e^{jk_z H}}{k_z (1 - e^{2jk_z H})} \quad (1.32)$$

$$Q_{22} = \omega_{2,kl}^2 - \omega^2 - \frac{j\omega\rho_0}{m_2} \frac{2\omega e^{2jk_z H}}{k_z (1 - e^{2jk_z H})} \quad (1.33)$$

$$F = \frac{2j\omega\rho_0 I_{kl}}{m_1} \quad (1.34)$$

The transmission coefficient of sound power is a function of the elevation angle  $\varphi$  and azimuth angle  $\theta$  of the incidence sound, which can be expressed as

$$\tau(\varphi, \theta) = \frac{\sum_{m=1}^{\infty} \sum_{n=1}^{\infty} |\xi_{mn}|^2}{\sum_{m=1}^{\infty} \sum_{n=1}^{\infty} |I_{mn} + \beta_{mn}|^2} \quad (1.35)$$

For diffuse incident sound, due to the symmetry of the rectangular double-panel structure, the averaged transmission coefficient can be obtained by integration as

$$\tau_{\text{diff}} = \frac{\int_0^{\pi/4} \int_0^{\varphi_{\text{lim}}} \tau(\varphi, \theta) \sin \varphi \cos \varphi \sin \theta \cos \theta d\varphi d\theta}{\int_0^{\pi/4} \int_0^{\varphi_{\text{lim}}} \sin \varphi \cos \varphi \sin \theta \cos \theta d\varphi d\theta} \quad (1.36)$$

where  $\varphi_{\text{lim}}$  is the limiting angle defining the diffuseness of the incident field. Here, a limited incident angle  $\varphi_{\text{lim}}$  is introduced to carry out this integration, inasmuch as it is picked to give a good fit with experiments [23, 37–41].

In order to describe the vibration intensity of the two panels as well as the local distribution of sound pressure, two parameters are introduced below [42]:

(1) Averaged quadratic velocity  $\bar{V}^2$ :

$$\bar{V}^2 = \begin{cases} \bar{V}_1^2 = \frac{\omega^2}{2A_1} \int |w_1|^2 dA \\ \bar{V}_2^2 = \frac{\omega^2}{2A_2} \int_{A_2} |w_2|^2 dA \end{cases} \quad (1.37)$$

where the subscripts 1 and 2 denote the incident panel and upper panel, respectively. For the present numerical calculations,  $\bar{V}^2$  will be plotted in decibel scale (dB) using a reference quadratic velocity of  $2.5 \times 10^{-15} \text{ m}^2/\text{s}^2$ .

(2) Averaged quadratic sound pressure  $\overline{P}^2$ :

$$\overline{P}^2 = \begin{cases} \overline{P}_1^2 = \frac{1}{2A_1} \int_{A_1} |p_1|^2 dA \\ \overline{P}_2^2 = \frac{1}{2A_2} \int_{A_2} |p_2|^2 dA \end{cases} \quad (1.38)$$

Here, only sound pressure in the near acoustic field (incidence field and radiating field) adjacent to each panel is considered, so the integration of Eq. (1.38) is taken over the panel area. Again,  $\overline{P}^2$  will be plotted in dB scale, with reference to  $4 \times 10^{-10} \text{ Pa}^2$ .

### 1.1.4 Convergence Check for Numerical Results

Numerical studies are performed to investigate the influence of relevant system parameters on the sound insulation property of simply supported double-panel partitions of finite extent, including the thickness of air cavity, panel dimensions, and the elevation and azimuth angles of incident sound. The material properties and structural dimensions of the panels are taken as follows. The two panels are made of aluminum, with Young's modulus  $E = 70 \text{ GPa}$ , density  $\rho = 2,700 \text{ kg/m}^3$ , Poisson ratio  $\nu = 0.33$ , and loss factor (damping)  $\eta = 0.01$ . The two rectangular panels have identical dimensions:  $a = 1.2 \text{ m}$  in the  $x$ -direction and  $b = 0.8 \text{ m}$  in the  $y$ -direction. Unless stated otherwise, the panels have thickness  $h = 2 \text{ mm}$ , while the thickness of the air cavity is fixed at  $H = 21.5 \text{ mm}$ . However, both  $h$  and  $H$  will be varied later to explore their influences on sound insulation. Air density is  $\rho_0 = 1.21 \text{ kg/m}^3$ , sound speed in air is  $c_0 = 343 \text{ m/s}$ , and the amplitude of the acoustic velocity potential for the incident sound is  $I_0 = 1 \text{ m}^2/\text{s}$ .

Since the analytical solutions are presented in the form of double series, a sufficiently large number of terms must be adopted to ensure the solution convergence. It is admissible that once the solution is convergent at a given frequency, it is also convergent for all frequencies lower than that [43], so that the necessary number of terms is determined by the highest frequency of interest. Here, without loss of generality,  $f = 6,000 \text{ Hz}$  is selected as the highest frequency for convergence checking. In the case when the incident sound is normal to the double-panel partition, the results shown in Fig. 1.2 demonstrate that the solution is rendered convergent if the single model number  $m$  (and  $n$ ) has a value of 50 or larger. This implies that at least 2,500 terms (with both  $m$  and  $n$  ranging from 1 to 50) are needed in all the present calculations.

Moreover, note that the loss factor of the air cavity in between the two panels is too low ( $=0.001$  approximately for air) to have a significant effect on STL especially when the depth of the air cavity is small. In other words, the discrepancy



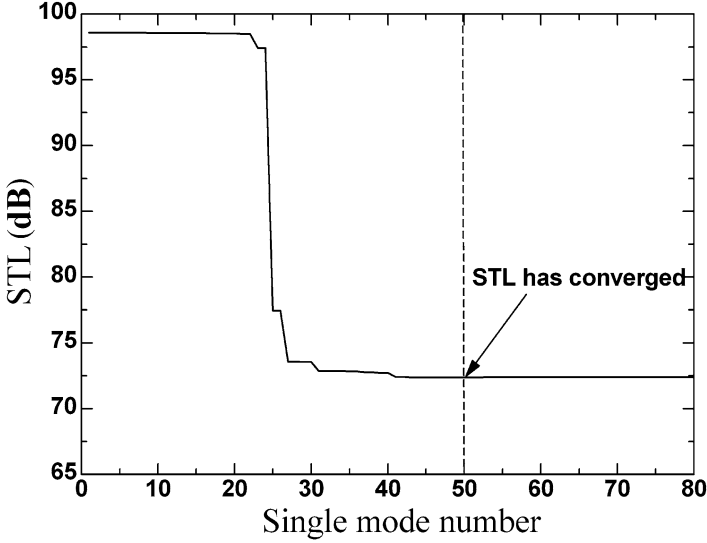


**Fig. 1.2** Convergence of double Fourier series solution for sound transmission loss (*STL*) of a double-panel partition under the excitation of a normally incident sound at 6,000 Hz (With permission from ASME)

between the predicted *STL* curve with air damping and that without air damping is invisible, owing to the negligible damping of the air. The real crucial matter is the vibroacoustic coupling behavior of the air cavity with the two panels, thus which will be elucidated in the following section in terms of several key system parameters (i.e., air cavity thickness, panel dimensions, the elevation and azimuth angles of incident sound).

### 1.1.5 Model Validation

For validation, the analytical solutions are compared with the existing experiment results [22], as shown in Fig. 1.3. A diffuse incident sound is assumed for the calculation of structural *STL*, with the structural dimensions and panel material properties same as those used in the experiment [22]. As mentioned above, an empirical value of the limiting elevation angle  $\varphi_{\text{lim}}$  is usually assumed. Although the empirical limit on the angle of field plane wave incidence may still be controversial, more and more researchers [23, 37–41] have acknowledged that the limiting angle falls within the range of 65–80° and prefer to adopt the angle of 78° for numerical analyses. Here, the results calculated with  $\varphi_{\text{lim}} = 65^\circ$  and 78°, respectively, are both presented in Fig. 1.3. It is seen from Fig. 1.3 that the theoretical predictions exhibit the same trend as the experimental measurements. Both the theoretical and experimental curves show two minima in the frequency range of concern, although

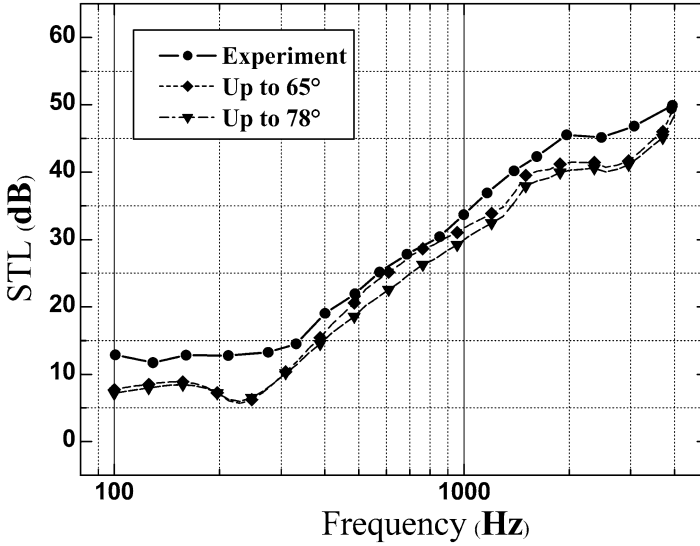


**Fig. 1.3** STL plotted as a function of frequency for a double aluminum panel ( $m_1 = m_2 = 0.239 \text{ g/cm}^2$ ,  $H$ ; diffuse incident sound): theory versus experiment [23] (With permission from ASME)

the first minimum on the experiment curve is only faintly observable. The first minimum at about 230 Hz corresponds to the mass-air-mass resonance related mainly to the low angles of incidence, while the second minimum appearing at the critical frequency of 2,546 Hz is mostly caused by the high angles of incidence, as mentioned by Villot et al. [23].

The experimentally measured STL values are consistently about 5 dB larger than the theoretically predicted values over the entire range of frequency studied (Fig. 1.3), which can be explained by the fact that glass fiber absorbent (several feet thick) was used around the edges of the double-panel partition in actual measurements. Otherwise, the theoretical predictions of Fig. 1.3 agree reasonably well with experiments.

To check the accuracy of the present model predictions further, another comparison is made with the theoretical and experimental results of Carneal et al. [26] for the case of normal incident sound (i.e.,  $\varphi = 0^\circ$ ), as shown in Fig. 1.4. The double-panel partition considered consists of two identical aluminum plates (0.38 m by 0.30 m, 1.6 mm thickness), separated by a 0.048 m air cavity. Again, a close agreement between the present theoretical predictions and experiment measurements is observed. Due to the experiments that were carried out by using two clamped parallel panels, as an approximation, Carneal et al. [26] increased the stiffness of the simply supported plate by a factor of  $\sqrt{2}$  for each boundary to approximate the clamped boundary condition; the present theoretical results in Fig. 1.4 adopts the same manner.

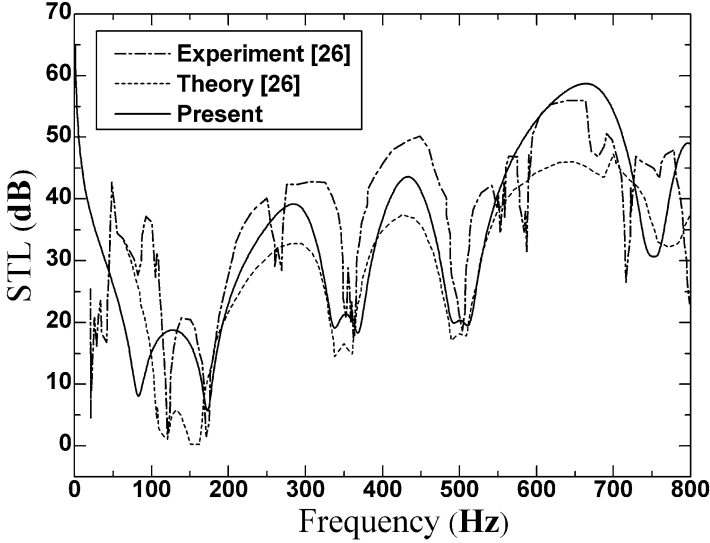


**Fig. 1.4** STL plotted as a function of frequency for a double aluminum panel with dimensions  $a = 0.38$  m,  $b = 0.30$  m, and  $H = 0.048$  m (normal incident sound): theory versus experiment [26] (With permission from ASME)

### 1.1.6 Effects of Air Cavity Thickness

Transmission of sound through a double-panel partition without any mechanical connection is due to the enclosed air between the two panels. Air in the cavity acts as springs, thus transmits the mechanical vibration of the incident panel to the radiating panel. The equivalent stiffness of the air between two parallel panels is given by Carneal and Fuller [26] and Fahy [30]:

$$K_a = \frac{\rho_0 c_0^2}{H} \quad (1.39)$$

The equivalent stiffness of the air is expected to have a significant effect on the sound transmission through the double-panel configuration. Therefore, it is necessary to investigate how the thickness of the air cavity influences the sound insulation capability of the structure.

With other geometrical dimensions of the structure fixed, the STL of the double-panel partition as a function of frequency is plotted in Fig. 1.5 for the case of normal incident sound and three selected values of air cavity thickness ( $H = 5.275$  mm, 21.5 mm, and 86 mm). It is seen from Fig. 1.5 that the first resonance frequency corresponding to the first minimum on the STL versus frequency curve decreases as  $H$  is increased, which is expected because increase of air cavity thickness leads to reduced equivalent air stiffness (Eq. 1.39). Overall, the curve is shifted toward the left with increasing  $H$  (Fig. 1.5), indicating that the sound insulation property of the partition is improved.

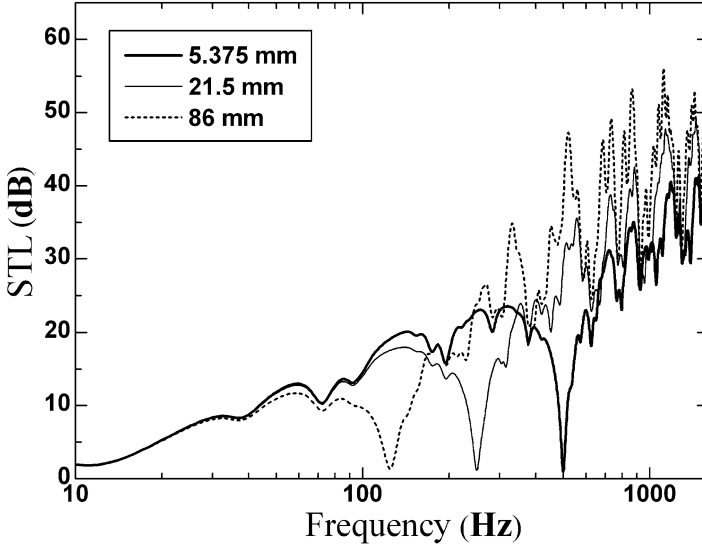


**Fig. 1.5** STL plotted as a function of frequency for double-panel partitions with different thicknesses of enclosed air cavity (normal incident sound) (With permission from ASME)

The vibroacoustic performance of the double-panel structure is also investigated in terms of the averaged quadratic velocity of the two panels (Fig. 1.6) and the averaged quadratic sound pressure field in the close proximity of the two panels (Fig. 1.7). The double-panel partition addressed is identical to that of Fig. 1.5. The increase of air cavity thickness reduces the vibroacoustic coupling of the structure due to weakened air pumping effects (equivalent stiffness effects), which is reflected by the decline of distinctions between the averaged quadratic velocity levels of the incident panel (Fig. 1.6a) and the radiating panel (Fig. 1.6b) as  $H$  is increased. It is understandable that a stronger vibroacoustic effect of the air cavity (with relatively small thickness) leads to enhanced transmission of vibration energy from the incidence panel to the radiating panel, and hence, the vibration energies of the two panels will be in closer agreement because of the less energy expense in the transmission process. As the averaged quadratic velocity is directly related to the vibration energy of the panel, similar vibration energy levels of the two panels will be reflected by similar averaged quadratic velocity levels (Fig. 1.6). It should be pointed out that the first maximum in the averaged quadratic velocity curve of the radiating panel in Fig. 1.6b corresponds to the first minimum on the STL curve in Fig. 1.5. That is also expected because the intensive vibration of the radiating panel would radiate sound strongly, sharply decreasing the magnitude of the STL.

The double-panel partitions with different thicknesses of air cavity are excited by the same incident sound of unit amplitude, i.e., the input sound energy is identical for the three cases studied in Figs. 1.5, 1.6, and 1.7. However, the vibration energy

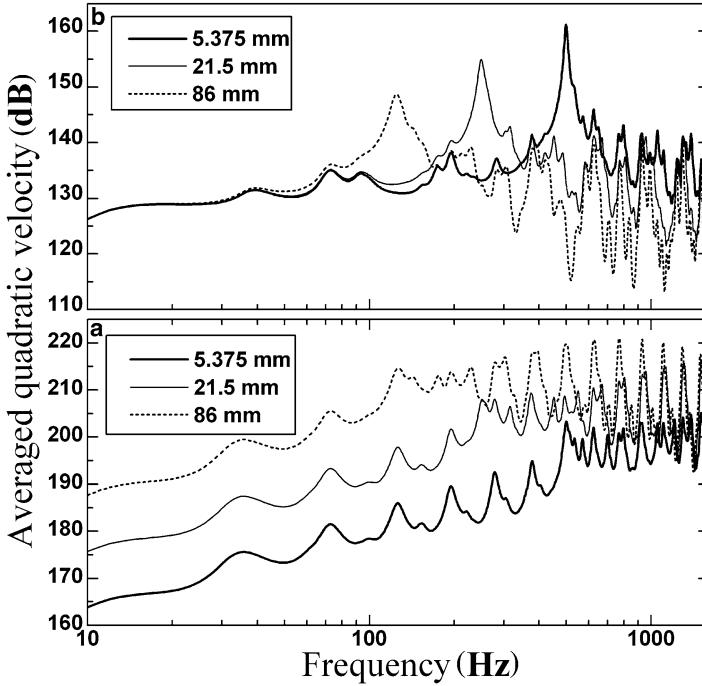


**Fig. 1.6** Averaged quadratic velocity plotted as a function of frequency for double-panel partitions with different thicknesses of enclosed air cavity (normal incident sound): (a) incidence panel; (b) radiating panel (With permission from ASME)

of the incident panel (as reflected by the average quadratic velocity, Fig. 1.6a) increases with the increase of air cavity thickness while that of the radiating panel decreases (Fig. 1.6b). This also demonstrates that the increase of air cavity thickness weakens the vibroacoustic coupling effect of the structure, inducing less energy transmitting through the air cavity. Although subjected to the same sound excitation, the noticeable differences appearing in the vibration levels of the incident panel for the three cases (see Fig. 1.6a) are attributed to the different vibroacoustic performances of the backed air cavities having different depths, while the sound energy fluxes penetrating through the air cavity to the radiating panel do not deviate so much because of the larger vibration level of the incident panel with a weaker cavity coupling (e.g., the 86 mm case) and the smaller vibration level of the incident panel with a stronger cavity coupling (e.g., the 5.375 mm case). As a result, the vibration levels of the radiating panel are almost the same at low frequencies; see Fig. 1.6b. Since the sound pressure level in the transmitted field completely stems from the vibration of the radiating panel, it should remain nearly unchanged at low frequencies; see Fig. 1.7. Finally, given the definition of the STL, it should be almost the same for the considered three cases at low frequencies. Therefore, the noticeable differences in the vibration level of the incident panel in Fig. 1.6a at low frequencies

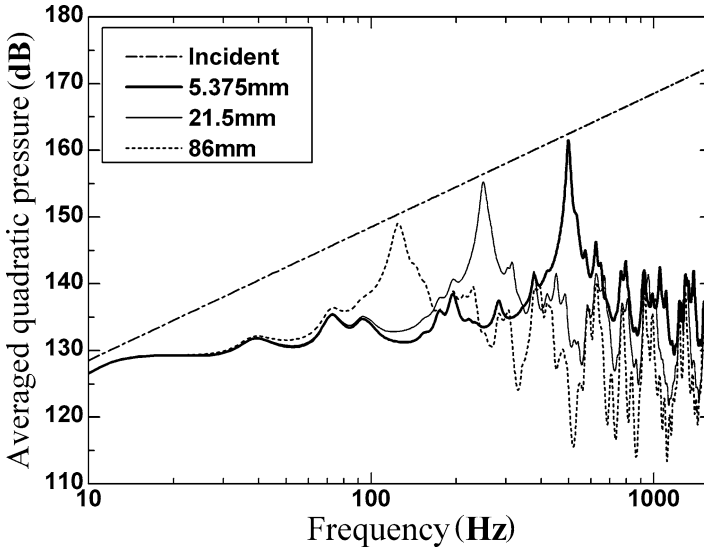


**Fig. 1.7** Averaged quadratic sound pressure plotted as a function of frequency for double-panel partitions with different thicknesses of enclosed air cavity (normal incident sound) (With permission from ASME)

do not exist in Figs. 1.5, 1.6, and 1.7. Of course, the maxima and minima shown in these figures represent the modal behaviors of the two panels and the air cavity.

It is interesting to observe from Fig. 1.6 that the frequencies where most of the maxima and minima appear remain unchanged (or slightly shifted) as  $H$  is varied, although the actual values of the averaged quadratic velocity at these frequencies may change significantly. The reason is that the incident and radiating panels are made of the same material, have the identical dimensions, and are both simply supported on their edges, and hence, the two panels have the same natural resonance frequencies (which are related to the vibration energy maxima). The slight shifting of the maxima (or minima) at certain frequencies (Fig. 1.6) should be attributed to the influence of the vibroacoustic coupling effects of the air cavity.

The influence of air cavity thickness  $H$  on the averaged quadratic sound pressure is shown in Fig. 1.7 for both the incident field and the radiating field. Although the excitation intensity is the same, the sound pressure level of the radiating acoustic field varies considerably as  $H$  is changed. Note that, for a given  $H$ , the averaged quadratic sound pressure of the radiating acoustic field (Fig. 1.7) is almost the same as the averaged quadratic velocity of the radiating panel (Fig. 1.6b). This is expected because the sound energy adjacent to the radiating panel is generated directly by the panel. For the same reason, the first maximum on the averaged quadratic sound pressure versus frequency curve (Fig. 1.6b) corresponds to the first minimum appearing in the STL versus frequency curve of Fig. 1.5. Finally, it should be pointed out that the incident sound pressure not only varies with time but also depends upon the incident frequency, as shown by the dash-dot curve in Fig. 1.7.